Statistics of approximately self-affine fractals: Random corrugated surface and time series

Rama Kant*
Condensed Matter Theory Unit, Jawaharlal Nehru Centre for Advanced Scientific Research, Bangalore 560 012, India
(Received 21 February 1995; revised manuscript received 10 January 1996)

Rough corrugated surfaces or time series are modeled as one-dimensional, stationary, Gaussian random processes with power-law power spectra over a limited range of frequencies and analyzed with the techniques of random processes. Surfaces with power-law spectra with small- and large-scale cutoffs exhibit approximate self-affine fractals behavior. There are two crossover scales, viz., a lower crossover scale and an upper crossover scale for nonfractal to fractal and fractal to nonfractal transition, respectively. We find the exact representation for the various statistical properties, viz., the mean square (MS) width, the MS slope, the MS curvature, the mean curve length (area), the mean zero crossing density the correlation function, and the structure function for these class of curves or corrugated surfaces. The importance of roughness exponent, upper and lower cutoff scales, and crossover of power-law spectra to non-power-law spectra to statistical properties of approximately self-affine fractal is emphasized. The scaling behavior of various statistical properties in the region between the two crossover scales is discussed. We suggest several methods for extracting fractal dimension. Finally, we apply our results to a granular flow experiment to characterize various time scales and gross statistical measure in this problem. [S1063-651X(96)06605-6]

PACS number(s): 05.40.+j, 02.50.Ey, 61.43.Hv

I. INTRODUCTION

Many natural and artificial surfaces and time series are disordered and have varying degree of randomness. Complexities in these systems arise either from geometric disorder or chemical disorder or both and in some cases it is from the dynamics of physical system. Disorder can be either fractal or nonfractal in nature. Fractal disorder is usually understood in terms of a self-similar or generally as a self-affine structure [1–11]. Statistical self-affine scaling systems can be viewed as random processes with power-law power spectra [1–5]. Here we are more specifically concerned with surfaces or time series with power spectra, given as

$$\langle|\hat{\zeta}(K)|^2\rangle = T|K|^{-2H-1}, \tag{1.1}$$

where $\hat{\zeta}(K)$ is the Fourier transform of random curve or surface profile $\zeta(x)$, K is the wave number, and T is related to the strength of the fractal. The angular brackets in Eq. (1.1) designate an ensemble averaging. H in the spectral exponent is the Hurst (or roughness) exponent and its values are restricted to the interval between 0 and 1. A curve or surface with the Hurst exponent (H) can be treated as a fractal curve or surface with (global) fractional dimensionality (D_H)

$$D_H = 2 - H, \tag{1.2}$$

where the fractional dimension of the curve or the curved side of the surface lies between 1 and 2. Curves with pure power-law frequency spectra i.e., ''ideal'' fractal structures, do not possess any characteristic scale. Power-law power spectra are known to give rise to fractal curves and surfaces with hierarchical structure possessing statistical scaling properties [3]. A wide variety of physical systems show power-law behavior in space (fractal) or time ($1/f^{\alpha}$ noise). Some examples are man-made surfaces [5], fracture the surfaces [12], electrodes [13], geographical terrains [1,5,14,15], surface of the moon [14], the ocean bottom [15], ocean waves spectra under various sea and atmospheric conditions [16], atmospheric turbulence [17], and stochastic time series [18–25]. $1/f^{\alpha}$ spectra can also arise from a deterministic chaotic physical system [23,26]. Similarly, in biological systems such as DNA, the spectral density of individual base positions has low-frequency power-law noise [27]. An important model for the random fractal power-law power spectra is the fractional Brownian motion [1,2,8]. It is therefore of great importance to understand various statistical properties of such power spectra.

An ideal fractal with a power-law spectrum is not a true representation of any physical surface or curve that possesses scaling properties only over a finite range of scales. A physically realistic power spectrum possesses both small- and large-scale cutoffs. Recently, Yordanov and Nicolaev have developed an important method for retrieving the parameters of such cutoff power-law spectra from experimentally recorded data [24].

In this paper we are concerned with the understanding of the statistical properties of the random Gaussian curves or surfaces with and without sharp cutoff power-law power spectra. The main results for the statistics of such approximately self-affine fractals are reported in Sec. II. This includes the cutoff power-law spectra (Sec. II A); expressions for the statistical properties such as the correlation functions and fractal crossover for approximate power-law spectra (Sec. II B); moments of power spectra e.g., mean square width and mean square slope (Sec. II C); probability distribution functions for height and its derivative for the approxi-

*Mailing address: Collège de France, Physique de la Matière Condensée, 11, Place Marcelin-Berthelot, 75231 Paris Cedex 05, France. Electronic address: kant@ext.jussieu.fr

mate power-law spectra, mean curve length, area, and curvature (Sec. II D); and zeros and persistence (Sec. II E). In Sec. III we compare our results with experimental observations for the granular flow and identify various time scales of this problems. Conclusions are reported in Sec. IV.

II. STATISTICAL PROPERTIES OF APPROXIMATELY SELF-AFFINE FRACTALS

Several decades ago Womersley and Hopkins [28] pioneered the use of random processes to describe rough surfaces. This method is now well established [29–35]. The common models for random surface texture or time series are statistically characterized by the power spectra, the correlation function, or the structure function of a centered, Gaussian random process [29–35]. These three statistical characteristics are related to each other. Moments of the power spectral density [29–31] are important for obtaining various statistical properties of the surface, e.g., the mean square (MS) width, the MS slope, the MS second (and higher) derivatives, their probability distribution functions, the mean area, the mean square value of the curvature, the zero crossing density, and the density of extremum points.

In this paper we deal with disorder that arises due to roughness about a plane surface (for a corrugated surface) or a line (for time series), the largest scale of disorder is taken to be much less than the linear size of the system. The surface corrugation or disorder is expressed as a continuous and single-valued random function $z=\zeta(x)$, which represents the (surface) elevation for all coordinate points (x). As mentioned above, the power spectrum is sufficient to characterize such centered, stationary, Gaussian surfaces or curves. The statistical properties of random corrugated surfaces or time series with nonfractal power spectra are usually well defined quantities, but for ''ideal'' fractals with power-law spectra Eq. (1.1) most of these quantities do not exist. For an assumed value of the spectral exponent, the Fourier transform and the moments of $\langle|\hat{\zeta}(K)|^2\rangle$ are divergent and thus the correlation function, variance, and MS derivatives do not exist. However, the structure function (SF) or mean square height increment function does exist and follows a self-affine scaling relation given by [3]

$$\langle[\zeta(x)-\zeta(x')]^2\rangle=\tau^{2(1-H)}X^{2H}, \tag{2.1}$$

where the angular brackets designate ensemble averaging and $X=|x-x'|$. Topothesy (τ) [3,5] is defined as the horizontal distance between two points on which the SF is equal to τ^2. Topothesy of an ideal fractal surface is related to the strength of the power-law spectra by the relation

$$\tau^{2(1-H)}=(T/\sqrt{\pi}H2^{2H})\Gamma(1-H)/\Gamma(1/2+H). \tag{2.2}$$

Surface profiles or time series functions that are statistically characterized by power-law spectra [see Eq. (1.1)] and power-law SFs [Eq. (2.1)] have a self-affine scaling property, viz.,, for a positive real b, $\zeta(bx)$ and $b^H\zeta(x)$ have identical SFs and therefore are statistically indistinguishable. As H increases or D_H decreases the fractal becomes smoother. Surfaces or curves with $H\to1$ and $H\to0$ are called marginal and extreme fractals [3], respectively. For a Brownian fractal surface, H and D_H are 1/2 and 1.5, respectively. The surfaces with $H<1/2$ or $D_H>1.5$ and $H>1/2$ or $D_H<1.5$ are ''super-Brownian'' fractals and ''sub-Brownian'' fractals, respectively.

It is important to emphasize that there is a profound difference between the power spectra of nonfractal and fractal structures. For a nonfractal (surface) there is a characteristic correlation length or time fixed by the rapidity of the fluctuation whereas for an ''ideal'' fractal (surface) there is no characteristic scale at all that can be seen from Eq. (1.1).

A. Power-law spectra with and without sharp cutoffs

Surfaces or time series that exhibit statistical self-resemblance over the entire range of scales can be described by the power spectra given by Eq. (1.1). However, any real surface or a time series is characterized by power-law spectra over a few decades in frequencies with a high- and a low-frequency cutoff [23]. The random surface or curve statistics can be approximated by power-law spectra with sharp frequency cutoffs or power-law spectra with low- and high-frequency crossover to non-power law spectra.

The power-law spectra with sharp wave-number cutoff are given as

$$\langle|\hat{\zeta}(K)|^2\rangle_{\mathrm{I}}=\begin{cases}0, & K<K_{\min}\\ T|K|^{-2H-1}, & K_{\min}\leqslant K\leqslant K_{\max}\\ 0, & K>K_{\max},\end{cases} \tag{2.3}$$

where $K_{\min}$ and $K_{\max}$ are low- and high-wave-number cutoffs, respectively. These approximate spectra may be suitable to understand statistical properties in the scaling region. The band limited power-law spectra in several cases show a gradual flattening for low wave numbers and a sharp decrease in non-power-law form for the high wave numbers. Such a power spectrum can be estimated by a function with a sharp flattening (white noise) at low wave numbers and a sharp cutoff at high wave numbers (i.e., power at high wave number is very small), which is given by

$$\langle|\hat{\zeta}(K)|^2\rangle_{\mathrm{II}}=\begin{cases}TK_{\min}^{-2H-1}, & K<K_{\min}\\ T|K|^{-2H-1}, & K_{\min}\leqslant K\leqslant K_{\max}\\ 0, & K>K_{\max}.\end{cases} \tag{2.4}$$

Similarly, an approximate power-law spectrum with sharp flattening at low wave numbers (white noise) and a gradual decrease at high wave numbers is given as

$$\langle|\hat{\zeta}(K)|^2\rangle_{\mathrm{III}}=\begin{cases}TK_{\min}^{-2H-1}, & K<K_{\min}\\ T|K|^{-2H-1}, & K_{\min}\leqslant K\leqslant K_{\max}\\ TK_{\max}^{-2H-1}\exp[-(K-K_{\max})/\beta K_{\max}], & K>K_{\max},\end{cases} \tag{2.5}$$

where β is the coefficient of correlation scale. The inset in Figs. 5 and 8 show plots of such power spectra with a large-wave-number nonfractal spectrum. This power spectrum has a sharp high-wave-number fall for small β and reduces to Eq. (2.4) for $\beta \to 0$. Similarly, for large β [in Eq. (2.5)] the power spectrum has a long high-frequency tail. These types of spectra can be used to estimate several experimental power spectra Refs. [51,50].

We define a surface or time series with sharp cutoff power-law spectra as a ''cutoff'' fractal. Apart from the fractal dimension, a fractal-like surface is characterized by three characteristic (length or time) scales: the large ($L_{\max}$) and small ($L_{\min}$) lateral cutoffs and a scale (l) that originates from the coefficient T of power spectra ($l^{2(1-H)}=T$) in Eqs. (2.3)–(2.5). The minimum wave number ($K_{\min}$) and maximum wave number ($K_{\max}$) are related to cutoff scales as $1/L_{\max}$ and $1/L_{\min}$, respectively. The range of (spatial) scales of the system is defined as

$$\rho = L_{\max}/L_{\min}. \tag{2.6}$$

It is an important characteristic in determining the relative importance of lower and upper cutoff scales. The fractal with finite $L_{\max}$ and $L_{\min} \to 0$ is called a ''finite'' fractal and one with $L_{\max} \to \infty$ and $L_{\min} \to 0$ is called an ''ideal'' fractal. The presence of lower and upper cutoff scales in the power spectra removes the divergences and make it a differentiable surface or a time series of finite variance. In the following section we analyze the correlation and structure function for an approximate power-law spectrum and their approximate self-affine scaling behavior, crossover scales, and the effect of the nonfractal high-frequency tail region.

B. Correlation functions, fractal crossover, and scaling exponent

In this section we obtain the exact expressions for the correlation function, difference correlation function, and effective scaling exponent for the various power spectra of Sec. II A. Their behavior in various regimes and the effect of crossover to low wave-number white noise spectra and high wave-number non-power-law behavior is analyzed.

The two-point correlation function for a statistically homogeneous surface is related to the power spectra by an inverse Fourier transform as

$$\langle \zeta(x)\zeta(x')\rangle = \frac{1}{2\pi}\int_{-\infty}^{\infty} dK e^{jKX}\langle |\hat{\zeta}(K)|^2\rangle, \tag{2.7}$$

where $j=\sqrt{-1}$ and $X=|x-x'|$. Substituting Eq. (2.3) in Eq. (2.7) we obtain the correlation function for the cutoff power-law spectrum, i.e., the real part (Re) of the expression

$$\langle \zeta(x)\zeta(x')\rangle_{\mathrm{I}} = \mathrm{Re}\left\{ \frac{T}{\pi}(-jX)^{2H}\Gamma\left(-2H, -\frac{jX}{L_{\max}}, -\frac{jX}{L_{\min}}\right)\right\}, \tag{2.8}$$

where $\Gamma(a,x_0,x_1)$ is the ''generalized'' incomplete gamma function, which is equal to $\Gamma(a,x_0)-\Gamma(a,x_1) = \gamma(a,x_1)-\gamma(a,x_0)$ [36]. The real part of Eq. (2.8) can be summed in terms of a (1,2) generalized hypergeometric function as

$$\begin{aligned}\langle \zeta(x)\zeta(x')\rangle_{\mathrm{I}} &= \langle \zeta(x)\zeta(x')\rangle_{\max} - \langle \zeta(x)\zeta(x')\rangle_{\min} \\ &= h_{\max 1}^2 F_2(-H;1-H,1/2,-(X/2L_{\max})^2) \\ &\quad - h_{\min 1}^2 F_2(-H;1-H,1/2,-(X/2L_{\min})^2),\end{aligned} \tag{2.9}$$

where $h_{\min}^2=(T/2\pi H)L_{\min}^{2H}$ and $h_{\max}^2=(T/2\pi H)L_{\max}^{2H}$.

The structure function or increment correlation function and the correlation function for a corrugated surface or a curve are related as

$$\Delta = \langle [\zeta(x)-\zeta(x')]^2\rangle = 2h^2 - 2\langle \zeta(x)\zeta(x')\rangle. \tag{2.10}$$

Substituting Eq. (2.8) in Eq. (2.10), we obtain

$$\Delta_{\mathrm{I}} = 2h^2 - 2\mathrm{Re}\left\{ \frac{T}{\pi}(-jX)^{2H}\Gamma\left(-2H, -\frac{jX}{L_{\max}}, -\frac{jX}{L_{\min}}\right)\right\}. \tag{2.11}$$

The real part of Eq. (2.11) can be summed in terms of a (1,2) generalized hypergeometric function as

$$\begin{aligned}\Delta_{\mathrm{I}} &= 2h_{\max}^2[1 - {}_1F_2(-H;1-H,1/2,-(X/2L_{\max})^2)] \\ &\quad - 2h_{\min}^2[1 - {}_1F_2(-H;1-H,1/2,-(X/2L_{\min})^2)].\end{aligned} \tag{2.12}$$

To determine the effect of two cutoff scales on the correlation functions we consider the various expansions for the correlation function at small, large, and intermediate separation scales.

Behavior of the correlation function for *small separation scales* is obtained by expanding the incomplete Γ functions [36] [Eq. (A1)] in Eq. (2.8) for small X. In this limit, the correlation function is

$$\begin{aligned}\langle \zeta(x)\zeta(x')\rangle_{\mathrm{I}} &= \frac{TL_{\max}^{2H}(1-\rho^{-2H})}{2\pi H} \\ &\quad - \frac{1}{\pi}\sum_{k=1}^{\infty}\frac{(-1)^{k+1}TL_{\min}^{2H}}{2(k-H)(2k)!} \\ &\quad \times \left(\frac{X}{L_{\min}}\right)^{2k}[1-\rho^{-2(k-H)}],\end{aligned} \tag{2.13}$$

where ρ is the ratio of cutoff length scales and is given by Eq. (2.6). In case of surfaces with $\rho \geqslant \max[5^{1/H}, 5^{1/(1-H)}]$ the contribution of ρ in each individual term is less than 4% and Eq. (2.13) simplifies to

$$\langle \zeta(x)\zeta(x')\rangle_{\mathrm{I}} = \frac{TL_{\max}^{2H}}{2\pi H} - \frac{1}{\pi}\sum_{k=1}^{\infty}\frac{(-1)^{k+1}TL_{\min}^{2H}}{2(k-H)(2k)!}\left(\frac{X}{L_{\min}}\right)^{2k}. \tag{2.14}$$

For $X \to 0$, in Eqs. (2.13) and (2.14), we obtain the MS width of the surface.

Similarly, we obtain the leading behavior of the SF for small separation scales to be

$$\Delta_{\mathrm{I}} = \frac{TL_{\min}^{2H}}{2\pi(1-H)}\left(\frac{X}{L_{\min}}\right)^2 + \cdots. \tag{2.15}$$

(See the small-X behavior of a representative plot of $\Delta_{\rm I}$ in Fig. 8.)

Similarly, in the *large separation scales*, i.e., $X \gg L_{\rm min}$ and $X > L_{\rm max}$, the asymptotic expansion of the incomplete Γ function [36] [see Eq. (A2)] in Eq. (2.8) gives

$$\langle \zeta(x)\zeta(x')\rangle_{\rm I} = h_{\rm max}^2 \sum_{k=1}^{\infty} (-1)^{k+1}(2H)_k \times \frac{\cos(X/L_{\rm max} + k\pi/2)}{(X/L_{\rm max})^k}, \qquad (2.16)$$

where $(2H)_k = \Gamma(2H+k)/\Gamma(2H)$ is the Pochammer's symbol for this ratio and $\Gamma(2H)$ is the gamma function. Equation (2.16) shows that the correlation function goes to zero in an oscillatory manner for large X.

Substituting Eq. (2.16) in Eq. (2.10), one can see that for large distances ($X \gg L_{\rm max}$) the effect of the $L_{\rm max}$ term is dominant and the SF shows its second asymptotic regime where it approaches $2h^2$ in an oscillatory manner as

$$\Delta_{\rm I} = 2h^2 - 4Hh_{\rm max}^2 \frac{\cos(X/L_{\rm min} + \pi/2)}{(X/L_{\rm min})} + \cdots. \qquad (2.17)$$

(See the large-X behavior of a representative plot for $\Delta_{\rm I}$ in Fig. 8.)

For *intermediate separation scales*, i.e., the approximate fractal regime $L_{\rm max} > X > L_{\rm min}$, an asymptotic expression for Eq. (2.8) is obtained by using the asymptotic expressions for the incomplete Γ function [36] [see expansions given by Eqs. (A1) and (A2)] as

$$\langle \zeta(x)\zeta(x')\rangle_{\rm I} = -\frac{\tau^{2(1-H)}}{2} X^{2H} + h_{\rm min}^2 \sum_{k=1}^{\infty} (-1)^k (2H)_k \times \frac{\cos(X/L_{\rm min} + k\pi/2)}{(X/L_{\rm min})^k} + h_{\rm max}^2 - h_{\rm max}^2 \sum_{k=1}^{\infty} \frac{(-1)^k H}{(k-H)(2k)!} \left(\frac{X}{L_{\rm max}}\right)^{2k}, \qquad (2.18)$$

where $\tau^{2(1-H)}$ is defined by Eq. (2.2).

Equation (2.11) for the structure function apparently does not exhibit self-affinity. The *approximate self-affinity* can be seen in the asymptotic expansion for a large range of length scales, i.e., $L_{\rm max} \gg X \gg L_{\rm min}$. The asymptotic expansion of Eq. (2.11) yields

$$\Delta_{\rm I} \approx \tau^{2(1-H)} X^{2H} - 2h_{\rm min}^2 \left[1 - 2H \frac{\cos(X/L_{\rm min} + \pi/2)}{(X/L_{\rm min})}\right] - h_{\rm max}^2 (H/1-H)(X/L_{\rm max})^2 \cdots. \qquad (2.19)$$

The structure function for an ideal fractal is given by Eq. (2.1), which is the leading term in Eq. (2.19). Equation (2.19) suggests an approximate self-affine behavior for a surface or a time series with a cutoff power-law spectra. The oscillations produced by the second term are noticeable only for surfaces with relatively large $h_{\rm min}^2$ and decreases with an increase in X. In Eq. (2.19), τ is the topothesy and for an ideal fractal, which is given by Eq. (2.2). The topothesy for an ideal fractal depends only on the Hurst exponent; however, for a cutoff fractal it depends on the Hurst exponent as well as on two cutoff length scales.

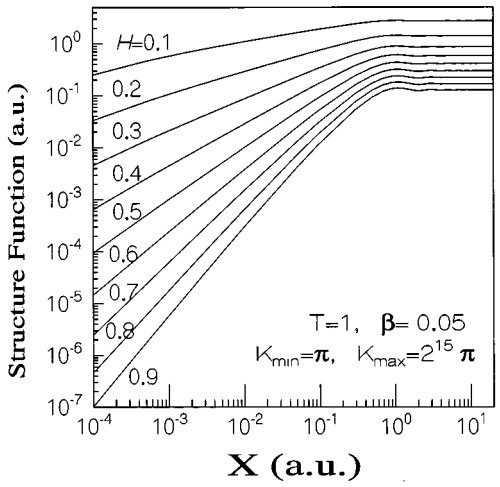

FIG. 1. Plot of the structure function $\Delta_{\rm III}(X,H)$ of Eq. (2.22) versus the spatial increment $X = |x - x'|$ for different values of the Hurst exponent H. The parameter values are the normalization constant $T = 1$ from Eq. (2.5), the coefficient of correlation scale $\beta = 0.05$ [see Eq. (2.5)], and wave-number cutoffs $K_{\rm min} = \pi$ and $K_{\rm max} = 2^{15}\pi$ defined in Eqs. (2.3)–(2.5). We see that the SF increases for the smaller values of H.

Similarly, the SF for the second power spectrum [Eq. (2.4)] is obtained as

$$\Delta_{\rm II} = \Delta_{\rm I} + \Delta_{\mathscr{L}}, \qquad (2.20)$$

where $\Delta_{\mathscr{L}}$ is given as

$$\Delta_{\mathscr{L}} = \frac{2TL_{\rm max}^{2H}}{\pi}\left[1 - \frac{\sin(X/L_{\rm max})}{X/L_{\rm max}}\right] \qquad (2.21)$$

and $\Delta_{\rm I}$ is given by Eq. (2.4). This SF include the contribution of low-wave-number white noise.

The SF for the third power spectrum [Eq. (2.5)] is

$$\Delta_{\rm III} = \Delta_{\rm I} + \Delta_{\mathscr{L}} + \Delta_{\mathscr{U}}, \qquad (2.22)$$

where $\Delta_{\mathscr{U}}$ is given by

$$\Delta_{\mathscr{U}} = \frac{2\beta TL_{\rm min}^{2H}}{\pi}\left[1 - \frac{\cos(X/L_{\rm min}) - \beta X \sin(X/L_{\rm min})/L_{\rm min}}{1 + (\beta X/L_{\rm min})^2}\right]. \qquad (2.23)$$

$\Delta_{\rm IV}$ is the SF for a power spectrum with a sharp lower cutoff and exponential higher-wave-number behavior. $\Delta_{\rm IV}$ is defined as

$$\Delta_{\rm IV} = \Delta_{\rm I} + \Delta_{\mathscr{U}}. \qquad (2.24)$$

[$\Delta_{\rm I}$, $\Delta_{\rm II}$, $\Delta_{\rm III}$, and $\Delta_{\rm IV}$ are plotted in Fig. 8 and are represented by curves (I), (II), (III), and (IV), respectively.]

In Fig. 1 we have plotted the SF ($\Delta_{\rm III}$; see Eq. (2.22)] for the various values of the Hurst exponent. In this figure we have taken the normalization constant $T = 1$, the coefficient of the correlation scale $\beta = 0.05$, and the wave-number cut-

offs $K_{\min}=\pi$ and $K_{\max}=2^{15}\pi$. We see that for a given value X, the value of the SF is higher for small roughness exponent. As we discussed earlier, qualitatively the SF can be classified in three categories: small-scale domain, approximately scaling intermediate-scale domain, and saturation behavior of a large-scale domain. These domains can be more clearly seen in the logarithmic derivative of the SF, which is discussed below.

In the following discussion we show the *scaling exponent* $\mathscr{H}(X,\rho)$ for the SF is not a global measure for all scales, viz., the scaling exponent is a function of X and cutoff scales. The function $\mathscr{H}(X,\rho)$ is obtained by taking the logarithmic derivative of the SF as

$$\mathscr{H}(X,\rho)=\frac{X}{2\Delta}\frac{d\Delta}{dX}. \tag{2.25}$$

The formula for the scaling exponent for the sharp cutoff power-law spectrum [Eq. (2.3)] is

$$\mathscr{H}_{\mathrm{I}}(X,\rho)=\frac{X}{2\Delta_{\mathrm{I}}}\frac{d\Delta_{\mathrm{I}}}{dX}. \tag{2.26}$$

Similarly, the scaling for the second power spectrum [Eq. (2.4)] is obtained as

$$\mathscr{H}_{\mathrm{II}}(X,\rho)=\frac{X}{2\Delta_{\mathrm{II}}}\left[\frac{d\Delta_{\mathrm{I}}}{dX}+\frac{d\Delta_{\mathscr{S}}}{dX}\right]. \tag{2.27}$$

This is the exact form for an approximate result obtained by Talocia [25].

The scaling exponent for the third power spectrum [Eq. (2.5)] is defined as

$$\mathscr{H}_{\mathrm{III}}=\frac{X}{2\Delta_{\mathrm{III}}}\left[\frac{d\Delta_{\mathrm{I}}}{dX}+\frac{d\Delta_{\mathscr{S}}}{dX}+\frac{d\Delta_{\mathscr{U}}}{dX}\right]. \tag{2.28}$$

Various derivatives or components in Eqs. (2.26)–(2.28) are defined below. The derivative of Δ_{I} is expressed as

$$\frac{d\Delta_{\mathrm{I}}}{dX}=-\frac{4H}{X}\langle\zeta(x)\zeta(x')\rangle_{\mathrm{I}}+\frac{2TL_{\max}^{2H}}{\pi X}\cos(X/L_{\max})-\frac{2TL_{\min}^{2H}}{\pi X}\cos(X/L_{\min}), \tag{2.29}$$

where the correlation function $\langle\zeta(x)\zeta(x')\rangle_{\mathrm{I}}$ is given by Eq. (2.8). The derivative of $\Delta_{\mathscr{S}}$ is obtained as

$$\frac{d\Delta_{\mathscr{S}}}{dX}=-\frac{2TL_{\max}^{2H}}{\pi X}\cos\left(\frac{X}{L_{\max}}\right)+\frac{2TL_{\max}^{1+2H}}{\pi X^2}\sin\left(\frac{X}{L_{\max}}\right). \tag{2.30}$$

Similarly, the derivative for $\Delta_{\mathscr{U}}$ is

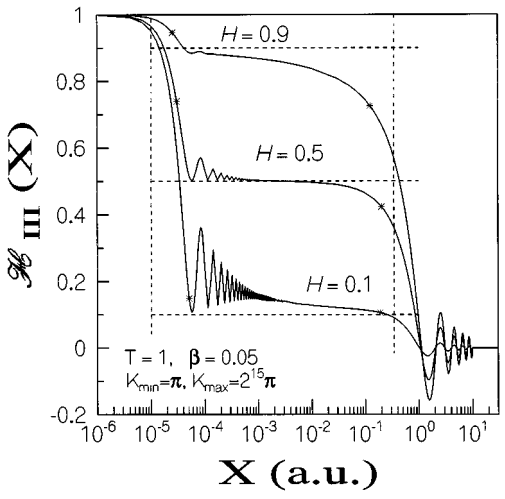

FIG. 2. Plot of the scaling exponent $\mathscr{H}_{\mathrm{III}}$ of Eq. (2.28) or the local slope of Δ_{III} versus the spatial increment $X=|x-x'|$ for three values of the Hurst exponent H. The parameter values are $T=1$, $K_{\min}=\pi$, $K_{\max}=2^{15}\pi$, and $\beta=0.05$ [see Eq. (2.5)]. Dotted vertical lines represent the positions of two cutoff scales and asterisk marks are the positions of the inner and outer crossover scales (see Eqs. 2.32 and 2.33). We see that the there is a systematic deviation in the value of the $\mathscr{H}_{\mathrm{III}}$ from the spectral exponent (represented by the horizontal dotted lines).

$$\frac{d\Delta_{\mathscr{U}}}{dX}=\frac{2\beta L_{\min}^{2H}T}{\pi\left(1+\frac{\beta^2X^2}{L_{\min}^2}\right)}\left(\frac{\beta X\cos\left(\frac{X}{L_{\min}}\right)}{L_{\min}^2}+\frac{(1+\beta)\sin\left(\frac{X}{L_{\min}}\right)}{L_{\min}}\right)+\frac{4\beta^3TXL_{\min}^{-2+2H}}{\pi\left(1+\frac{\beta^2X^2}{L_{\min}^2}\right)^2}\left(\cos\left(\frac{X}{L_{\min}}\right)-\frac{\beta X\sin\left(\frac{X}{L_{\min}}\right)}{L_{\min}}\right). \tag{2.31}$$

In Fig. 2 we have shown the scale dependence of the scaling exponent $\mathscr{H}_{\mathrm{III}}(X,\rho)$ [see Eq. (2.28)] for the same set of parameters as in Fig. 1. The scaling exponent that is obtained by a logarithmic derivative of the SF is very sensitive to small oscillations in the SF. In Fig. 1, for the SF, there is no perceptible oscillation for small-X behavior, but these oscillations are seen very clearly in the $\mathscr{H}_{\mathrm{III}}(X,\rho)$ plot. At very small scale (i.e., $X<L_{\min}$), $\mathscr{H}_{\mathrm{III}}(X,\rho)$ goes to unity and as X increases (i.e., $X>L_{\min}$) it approaches an approximately constant value close to the spectral exponent H in an oscillatory manner. Similarly, for $X>L_{\max}$, $\mathscr{H}_{\mathrm{III}}(X,\rho)$ goes to zero in an oscillatory manner. For $H=0.5$ or close to it, fairly accurate self-affinity is observed between the two crossover scales. This is not observed for H close to 1 and 0 (for a finite range of scale). There is a systematic deviation in the value of the scaling exponent, viz., the scaling exponent is underestimated and overestimated for the spectral exponent H close to 1 and 0, respectively. The dotted vertical lines indicate the position of lower and upper scale cutoffs. The asterisks in Fig. 2 mark the positions of the inner and outer crossover scales, which are defined below.

The *crossover scales* within which the surface shows approximate self-affinity can be roughly estimated by the limiting behavior. The *inner crossover scale* (L_i) is obtained by equating the leading term in Eqs. (2.15) and (2.19). L_i is given by

$$L_i \approx \chi_i L_{\min},$$

$$\chi_i = 2[\sqrt{\pi}\Gamma(2-H)/2H\Gamma(\tfrac{1}{2}+H)]^{1/(2-2H)}. \quad (2.32)$$

The inner crossover scale is a monotonically decreasing function of H. It is always greater than the lower cutoff length scale. The inner crossover scale is large for a small roughness exponent and decreases with an increase in the Hurst exponent, e.g., $L_i \to \infty$ for $H \to 0$, $L_i = \pi L_{\min}$ for $H = \frac{1}{2}$, and $L_i \to e^{3/2} e^{-\gamma} L_{\min} \approx 2.52 L_{\min}$ for $H \to 1$, where γ is a Euler constant.

The *outer crossover scale* (L_0) is obtained by equating the leading term in Eqs. (2.17) and (2.19). L_o is given by

$$L_o \approx \chi_o L_{\max},$$

$$\chi_o = 2[\Gamma(1/2+H)/\sqrt{\pi}\Gamma(1-H)]^{1/2H}. \quad (2.33)$$

The outer crossover scale (L_o) is not a monotonic function of the Hurst exponent. It has a maximum at $H \approx 0.38$ and is approximately equal to $0.65 L_{\max}$. The outer crossover scale for $H \to 0$ is given by $L_o \to e^{-\gamma} L_{\max} \approx 0.56 L_{\max}$; for $H = 1/2$ by $L_o = 2/\pi L_{\max} \approx 0.64 L_{\max}$; and for $H \to 1$ by $L_o \to 0$.

The ratio of the outer and inner crossover scales is the *range* (ρ_f) *of fractality*. ρ_f is proportional to ρ,

$$\rho_f = \chi \rho.$$

The proportionality constant $\chi = \chi_o / \chi_i$ in the preceding equation is given as

$$\chi = \left(\frac{\Gamma(H+\frac{1}{2})}{\sqrt{\pi}\Gamma(1-H)} \right)^{1/2H} \left(\frac{2H\Gamma(\frac{1}{2}+H)}{\sqrt{\pi}\Gamma(2-H)} \right)^{1/2(1-H)}. \quad (2.34)$$

Figure 3 shows the plot of logarithm of $1/\chi$, which is a measure of difference in decades of the range of cutoff scales and the range of fractality, versus the Hurst exponent H. This figure suggests that the spectral exponent H around 0.6 yields a broader scaling region than around 0 and 1. This figure also suggests that the range of fractality is always less than the range of cutoff length scales and the range of fractality has a maximum for $H \approx 0.59$ with $\rho_f \approx 0.21\rho$. The range of fractality falls on either side of the maximum and is zero for both marginal and extreme fractals. Therefore, a surface or time series with a small or large Hurst exponent should have a large ρ to show fractality over a finite range.

The above discussion also suggests that it is easier to form a scaling surface with an intermediate value of H. So one expects a frequent occurrence of a fractal surface with an intermediate value of the roughness exponent and a rare occurrence of a marginal or an extreme fractal surface. A similar conclusion can be drawn from Sayles and Thomas's [5] work, where they plot the histogram for the distribution of the roughness exponent of a variety of natural and artificial surfaces.

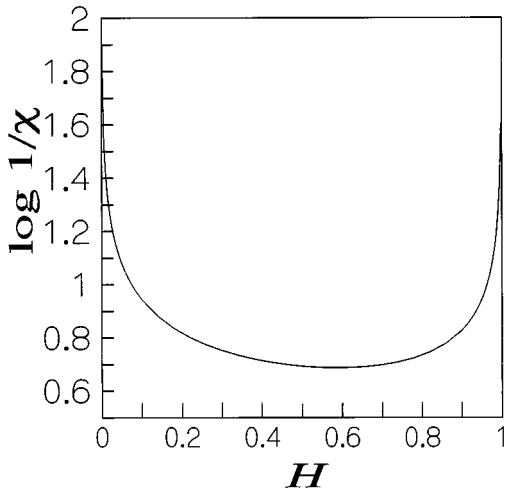

FIG. 3. Plot of $\log_{10} 1/\chi$ versus the Hurst exponent H. This shows the dependence of the difference in the decades of the range of cutoff scales and the range of fractality on the Hurst exponent [see Eq. (2.34)]. The difference diverges as $H \to 0$ or $H \to 1$ and is minimum around $H = 0.6$.

Figures 4(a) and 4(b) explore the scaling exponent dependence on the range of cutoff scales (ρ). The value of various parameters are the same as in Fig. 1. The scaling exponent approaches a stable fixed value near the geometric mean position of two crossover lengths viz., $X_m = \sqrt{L_i L_o}$. These figures show the systematic deviation in scaling exponent, $\mathcal{H}(X_m, \rho)$ i.e., for $H > 0.6$ we have $\mathcal{H}(X_m, \rho) < H$ and for $H < 0.6$ it follows the $\mathcal{H}(X_m, \rho) > H$. For systems with a broad range of scales we have an approximate identity $\mathcal{H}_{\rm III} \approx H$, which is valid only for the intermediate values of H, i.e., for $\rho > 10^3$; it is applicable for $0.4 \leqslant H \leqslant 0.6$. For these values of H one can ignore finite scale corrections i.e., Eq. (2.1) can be used to estimate the roughness exponent in the scaling region. These figures also show a very slow convergence of $\mathcal{H}(X, \rho)$ towards the expected values of $\mathcal{H}(X_m, \rho) = 0$ and 1 for $H = 0$ and 1, respectively. This is also observed in the numerical calculation of Osborne and Provenzale [19] and Higuchi [20].

For an ideal fractal or a random curve with pure power-law spectra [Eq. (1.1)], the fractal dimension linearly depends on the spectral exponent or spectral Hurst exponent, but the same is not true for a finite bandwidth power-law spectra. Figure 2 shows the scale dependence of $\mathcal{H}(X, \rho)$. Similarly, Fig. 4 shows the non-linear dependence of the fractal dimension on the roughness exponent (H) for a band-limited power law. Random processes with a band-limited power-law spectrum for a given spectral exponent (H) has a scale-dependent effective scaling exponent ($\mathcal{H}_{\rm eff}(X, \rho)$) that is related to the effective fractional dimensionality ($D_{\rm eff}(X)$) between two crossover scales as

$$D_{\rm eff}(X, \rho) = 2 - \mathcal{H}_{\rm eff}(X, \rho). \quad (2.35)$$

From Figs. 4(a) and 4(b) one can see that the effective scaling exponent for $\rho \leqslant 10^{10}$ approximately follows the inequality

$$0.04 \leqslant \mathcal{H}_{\rm III} \leqslant 0.96, \quad (2.36)$$

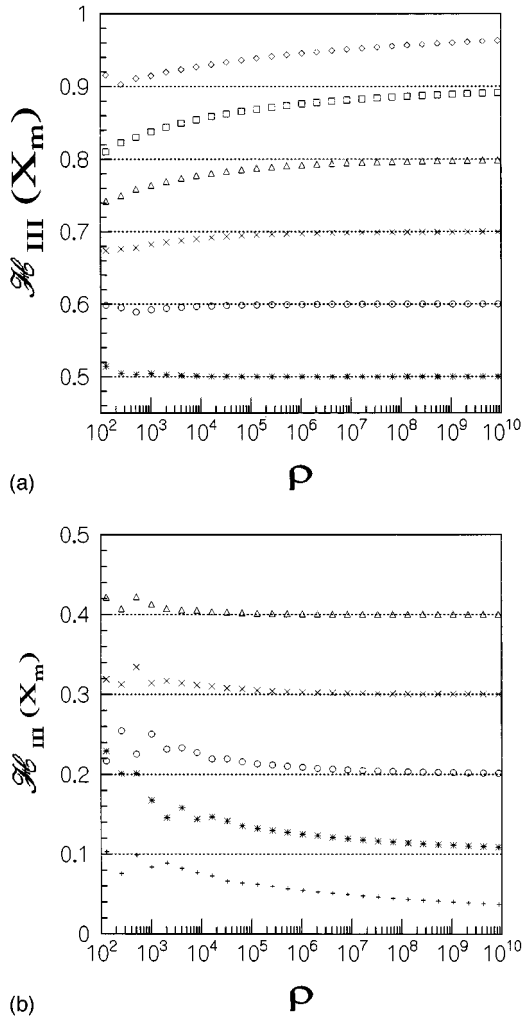

FIG. 4. Plot of the scaling exponent $\mathscr{H}_{\mathrm{III}}(X)$ and its dependence on the range of cutoff scales ρ [defined by Eq. (2.6)]. The parameter values are $T=1$, $\beta=0.05$, $K_{\min}=1/\pi$, and $K_{\max}=\rho K_{\min}$. (a) $H=1,0.9,\ 0.8,0.7,0.6$, and 0.5; (b) $H=0,0.1,0.2,\ 0.3$, and 0.4. For the (spectral) Hurst exponent (H) close to 0 and 1, $\mathscr{H}_{\mathrm{III}}$ has extremely slow convergence. It has systematic deviation with opposite trends around $H=0.6$.

though the spectral H varies between 0 and 1. The effective fractional dimension (D_{eff}) of the approximately fractal curve of finite range varies between 1.04 and 1.96. Similar conclusions are obtained for the fractal dimension of signals with $1/f^{\alpha}$ by Higuchi [20], Talocia [25], Labate *et al.* [38], and Fox [39] using different algorithms. We have tried to explain this using the exact result for the scaling exponent Eq. (2.28) (see Fig. 4).

An important measure to quantify the complexity of a chaotic dynamic system is the Grassberger-Procaccia [40] correlation dimension, i.e., $1/H$. This dimension of the strange attractor counts the effective number of degree of freedom in the dynamical system. Osborne and Provenzale [19] observed that the numerical estimate of the Grassberger-Procaccia correlation dimension [40] has a *finite* value even for a arbitrarily long time series. This finiteness of the correlation dimension is supported by our exact calculation in Fig. 4, where effective correlation dimension is $1/\mathscr{H}_{\mathrm{eff}}$.

Figure 5 shows the effect of the large-frequency crossover

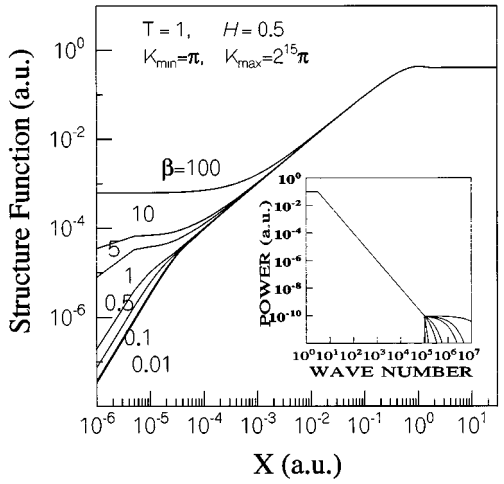

FIG. 5. Plot of the structure function $\Delta_{\mathrm{III}}(X,H)$ of Eq. (2.22) versus the spatial increment $X=|x-x'|$ for different values of the coefficient of correlation scales. The parameter values are $T=1$, $H=0.5$, $K_{\min}=\pi$, and $K_{\max}=2^{15}\pi$ and β is taken as 0.01, 0.1, 0.5, 1, 5, 10, and 100. The inset show the power spectra for various values of the correlation coefficient [see Eq. (2.5)]. We see that the size of scaling region reduces with an increase in the nonfractal tail region of the spectra.

nonfractal region of the power spectrum on the statistical scaling properties of the SF. The inset in Fig. 5 is a plot for the power spectra of Eq. (2.5) for several values of the correlation coefficient (β). The values of the parameters used in this figure are $T=1$, $H=0.5$, $K_{\min}=\pi$, and $K_{\max}=2^{15}\pi$ and the values of the correlation coefficient are 0.01, 0.1, 0.5, 1, 5, 10, and 100. In the inset the longest tail spectrum corresponds to $\beta=100$, the shortest tail spectrum corresponds to $\beta=0.01$, and other values of the spectra fall in between. The presence of a long tail in the power spectrum, i.e., $\beta=100,10$, or 5, destroys the scaling region of the SF. This means that the band-limited power-law spectrum is not a sufficient condition to make a scaling surface or time series, i.e., one needs to have a short tail high-wave-number non-power-law spectra.

A recent work of Yordanov and Nickolaev [24] is closely related to some of the work reported in this section. Yordanov and Nickolaev [24] have developed a method for determining the spectral parameters of experimentally recorded self-affine time series and they obtained an expression for the SF and the crossover time for the time series with a sharp cutoff power-law spectra. Our results, are consistent with their results, though their SF differs from ours [Eq. (2.12)] by a factor of $1/\pi$. This is because their [24] analysis is in half-space and uses a different definition for the Fourier transform. In the following sections we report and analyze exact mathematical formulas for the various other important statistical properties of band-limited power-law spectra that are or can be used to understand approximately self-affine fractals.

C. Moments of power spectra and significance of cutoff scales

The presence of a low frequency cutoff to $1/f^{\alpha}$ random processes makes it a finite power random processes. Similarly, the presence of an upper frequency cutoff in the power-

law power spectrum makes it a differentiable random process, which opens up the possibility of using derivatives of random processes to extract the fractal exponent. These (MS) derivatives are also important in defining the mean length of the curve, the MS curvature, the mean zero density, the mean density of extremum points, etc. A related work in Ref. [20] obtained the exponent in terms of the spectral exponent for the mth-order forward difference operation to a time series. In this section we obtain the exact results for the MS fluctuations and arbitrary MS derivatives and analyze their dependence on the scaling exponent and cutoff scales.

The variance and various mean square derivatives of a homogeneous random corrugated surface are related to the even moments (m_{2r}) of the power spectra. It is important to note that the odd moments of the power spectra are zero.

The zeroth moment ($r=0$) of the power spectrum has an important physical significance as it is the measure of the surface width, i.e., variance (h^2). This is one of the most utilized methods to extract the fractal dimension. The mean square width of the cutoff fractal can be represented in the form

$$m_0^{\mathrm{I}}=h^2=\frac{l^2(1-\rho^{-2H})}{2\pi H}\left(\frac{L_{\max}}{l}\right)^{2H}, \tag{2.37}$$

where l and T are related through $T=l^{2(1-H)}$. For a sufficiently wide range of frequencies, the leading contribution to the surface width comes from the upper cutoff length scale. The surface width decreases with a decrease in the range of spatial length scales. For $H\to 0$ (the extreme fractal), Eq. (2.37) corresponds to a surface with logarithmic roughness and the mean square surface width is equal to $l^2\ln\rho/\pi$. For a time series, the MS width is usually defined in such a way that it is equal to one-half of the MS width defined by us.

At this point we find the range (ρ_0) for the surface width above which one can ignore the effect of smaller length scales. This is estimated by taking $\rho_0^{-2H}=1/25$, from which

$$\rho_0=5^{1/H}. \tag{2.38}$$

ρ_0 increases exponentially as the roughness exponent decreases. This range ρ_0 is infinite for the extreme fractal and 5 for the marginal fractal. This implies that inclusion of a lower cutoff in the power-law spectra is more important for surfaces or time series with a small roughness exponent.

For curves or surfaces with $\rho\geqslant\rho_0$, the dimensionless width $h^2_{\max}/l^2$ is a nonmonotonic function of the roughness exponent and has a critical roughness exponent (H_0). The dimensionless MS width is minimum at H_0 and this critical roughness exponent is obtained in terms of $L_{\max}$ and l as

$$H_0=\frac{1}{2\,\ln(L_{\max}/l)}. \tag{2.39}$$

The magnitude of H_0 is solely decided by the upper cutoff scale and the strength of the fractal. The nonmonotonic behavior disappear for the fractals with range less than $\sqrt{l/L_{\min}}$ and they are a monotonically decreasing function of H.

In Fig. 6 we plot m_0^{I} [see Eq. (2.37)] with respect to H to show the range-dependent monotonic to nonmonotonic transition in the MS width. The parameters used in these plots

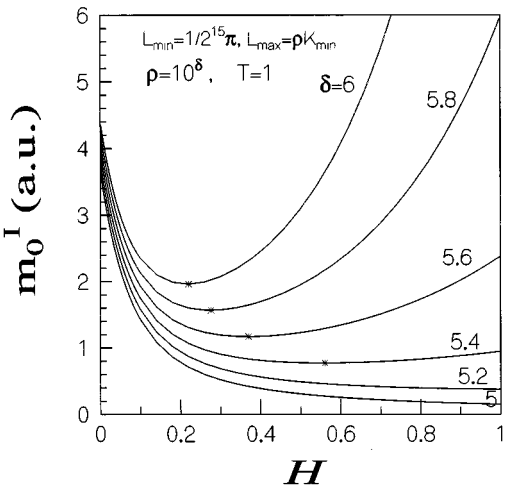

FIG. 6. Plot of the MS width m_0^{I} [Eq. (2.37)] versus Hurst exponent H for various values of range of cutoff scales ($\rho=10^{\delta}$). The parameter values are the normalization constant $T=1$ and the scale cutoffs $L_{\max}=10^{\delta}L_{\min}$ and $L_{\min}=1/2^{15}\pi$, where δ is taken as 6, 5.8, 5.6, 5.4, 5.2, and 5. Asterisks in the figure represent the positions of H_0 [see Eq. (2.39)]. We show that the minimum of the MS width becomes sharper and shifts toward the lower value of H with the increase in ρ.

are : $T=1$, $L_{\min}=1/2^{15}\pi$, and $L_{\max}=\rho L_{\min}$. Asterisks in the figure represent the positions of H_0 defined by Eq. (2.39). The monotonic to nonmonotonic transition occurs at $\rho\approx 10^{5.23}$. The MS width less than this range is a monotonically decreasing function of H. The minimum of the MS width become sharper and shifts towards the lower value of H with an increase in ρ. It will be interesting to verify this monotonic to nonmonotonic transition by numerically simulated data.

The second moment of power spectra (MS slope) is another important surface characteristic. It is needed for obtaining expressions for mean curve length, MS curvature, mean zero crossing density, and mean extremum density, and for cutoff fractals it is found to be

$$m_2^{\mathrm{I}}=\left\langle\left(\frac{\partial\zeta(x)}{\partial x}\right)^2\right\rangle=\frac{1-\rho^{-2(1-H)}}{2\pi(1-H)}\left(\frac{l}{L_{\min}}\right)^{2(1-H)}. \tag{2.40}$$

For marginal fractals the MS slope increases logarithmically with the range of roughness and is equal to $\ln\rho/\pi$. The rms slope increases in the power-law form with a decrease in the lower cutoff scale and also decreases with the decrease in ρ. The range ρ_1 (above which the effect of upper cutoff scale is not significant) for m_2 is given by

$$\rho_1=5^{1/(1-H)}. \tag{2.41}$$

The range ρ_1 for a Brownian fractal is 25. Similarly, the ρ_1's are 5 and ∞ for extreme and marginal fractal, respectively. Hence the inclusion of $L_{\max}$ in the power-law spectra is more important for surfaces with a higher Hurst exponent.

For surfaces with $\rho\geqslant\rho_1$, the MS slope m_2^{I} is a nonmonotonic function of H and has a critical roughness exponent (H_1). The MS slope has a minimum at H_1 and is given by the relation

$$H_1 = 1 - \frac{1}{2\ \ln(l/L_{\min})}\ . \tag{2.42}$$

The magnitude of H_1 is solely decided by the lower cutoff scale and the strength of the fractal. The MS derivative (m_2) shows a scaling property between two crossover length scales and is given by

$$m_2 = [1/2\pi(1-H)](l/L)^{2(1-H)}, \tag{2.43}$$

where L is an arbitrary length scale and is restricted between L_i and L_o, and $L_{\max}/L \geqslant \rho_1$.

In general, the $2r$th moment of the power spectra for a statistically homogeneous cutoff fractal is well defined and is given by

$$m_{2r}^{\mathrm{I}} = [T/2\pi(r-H)][L_{\min}^{-2(r-H)} - L_{\max}^{-2(r-H)}]. \tag{2.44}$$

Equation (2.44) shows that the importance of the upper cutoff scale decreases with an increase in the order of the moment. The contribution of the upper cutoff length scale is insignificant for higher surface moments. In the ideal or finite fractal limit the second and higher ($r>1$) moments diverge so the surface is nondifferentiable.

The presence of lower and upper non-power-law behavior in the spectrum modifies the $2r$th moment by extra additive terms. The $2r$th moment of the second power spectrum [see Eq. (2.4)] is

$$m_{2r}^{\mathrm{II}} = m_{2r}^{\mathrm{I}} + m_{2r\mathscr{L}}. \tag{2.45}$$

Similarly, the $2r$th moment for the third power spectrum [see Eq. (2.5)] is

$$m_{2r}^{\mathrm{III}} = m_{2r}^{\mathrm{I}} + m_{2r\mathscr{L}} + m_{2r\ \mathscr{U}}, \tag{2.46}$$

where $m_{2r\mathscr{L}}$ and $m_{2r\mathscr{U}}$ are given by

$$m_{2r\mathscr{L}} = TL_{\max}^{2(H-r)}/(1+2r)\pi \tag{2.47}$$

and

$$m_{2r\mathscr{U}} = (T/\pi)\beta^{1+2r}e^{1/\beta}L_{\min}^{2(H-r)}\Gamma[1+2r,1/\beta]. \tag{2.48}$$

The mean square rth derivative has a scaling property for an arbitrary length scale L and is given by

$$m_{2r} = [T/2\pi(r-H)]1/L^{2(r-H)}, \tag{2.49}$$

where $L_i < L < L_o$ and $L_{\max}/L \geqslant \rho_r$ ($=5^{1/(r-H)}$). The rth MS derivative of $\zeta(x)$ leads to a shift in exponent by $2r$.

D. Probability densities, curve length, and curvature

Physical surfaces or time series described by stationary random processes and in the absence of long-range correlations (and with finite variance) are expected to show Gaussian behavior. Gaussian behavior arises from the central limit theorem [30,37].

For an ideal self-affine surface fractal the variance, slope, and higher derivatives do not exist, so the application of the central limit theorem for these properties is ruled out. For an approximately self-affine fractal, however, these quantities are finite and the central limit theorem is applicable. The probability density and joint probability for the surface elevation, slope, and other higher derivatives are distributed according to the normal law. This can be shown by representing the surface elevation by a sum of a large number of sinusoids with random phases whose coefficients are decided by the power spectral density [19,29–31]. The Gaussian distribution of surface elevation has been measured for various surface corrugations [33].

The probability density for the elevation can be obtained by substituting an appropriate expression for m_0 [e.g., Eqs. (2.37), (2.45), (2.46)] in a Gaussian distribution. The width of the Gaussian function increases with an increase in $L_{\max}$ and ρ. Between the two crossover length scales and for $L/L_{\min} \geqslant \rho_0$, the probability density shows scaling behavior and is given by

$$p(\zeta,L) = (H/TL^{2H})^{1/2}\exp(-2\pi H\zeta^2/TL^{2H}). \tag{2.50}$$

Equation (2.50) has the scaling property

$$p(\zeta^* = b^H\zeta, L^* = bL) = b^{-H}p(\zeta,L). \tag{2.51}$$

Another important quantity is the probability density function of the slope $p(\xi_1)$, which is represented as

$$p(\xi_1) = e^{-\xi_1^2/2m_2}/\sqrt{2\pi m_2}. \tag{2.52}$$

The probability density for the slope is obtained by substituting the appropriate expression for m_2 [e.g., Eqs. (2.40), (2.45), and (2.46)] in Eq. (2.52). The probability density for the cutoff fractal has a scaling property between two crossover scales for $L_{\max}/L \geqslant \rho_1$ and is given by

$$p(\xi_1^* = b^{-(1-H)}\xi_1, L^* = bL) = b^{(1-H)}p(\xi_1,L). \tag{2.53}$$

The *contour length* of the fractal curves [41] are used to obtain the fractal dimension by Higuchi [18,20] and Osborne and Provenzale [19]. In the following discussion we obtain exact results for the contour length and study their scaling and nonscaling regimes. The contour length of the curved side of a corrugated surface or a time series is given by

$$\Gamma = \int_{\Gamma_0}\left[1 + \left(\frac{\partial\zeta(x)}{\partial x}\right)^2\right]^{1/2} dx, \tag{2.54}$$

where Γ_0 is the average line about which the curved side of the surface is fluctuating. The probability density function for the slope [Eq. (2.52)] is used to obtain the exact expression for the mean contour length, which is given by

$$\langle\Gamma\rangle = \sqrt{A_0/2m_2}\,\mathscr{U}(1/2,2,1/2m_2), \tag{2.55}$$

where $\mathscr{U}(a,b,z)$ is a confluent hypergeometric function [36], $\sqrt{A_0}$ is the length of the line Γ_0, and A_0 is the (macroscopic) area of the surface. The mean area and mean contour length are related through:

$$\langle A\rangle = \sqrt{A_0}\langle\Gamma\rangle. \tag{2.56}$$

The roughness factor (R^*) is the dimensionless mean contour length or mean area of the rough surface and is defined as

$$R^*=\langle A\rangle/A_0\equiv\langle\Gamma\rangle/\sqrt{A_0}=(1/\sqrt{2m_2})\,\mathscr{U}(1/2,2,1/2m_2). \tag{2.57}$$

The R^* increases with the second moment of the power spectra (m_2) of the surface.

To see the effect of m_2 on the roughness factor we expand Eq. (2.57) for small and large m_2. A small-m_2 asymptotic expansion implies that the roughness factor tends to 1 with decreasing m_2. Similarly, the large-m_2 expansion is obtained using the small argument [42] expansion for $\mathscr{U}$ [see Eq. (A4)] in Eq. (2.57). The leading term in R^* goes as $\sqrt{m_2}$ and higher order terms have both power-law and logarithmic dependences on m_2. R^* for $m_2\gg 1$ (i.e., large roughness surfaces) is obtained as

$$R^*\approx\sqrt{2m_2/\pi}. \tag{2.58}$$

To find the accuracy of this result we compare (numerically) it with an exact result for the roughness factor given by Eq. (2.57). Equation (2.58) underestimates the roughness factor: the deviation involved in this approximation for surfaces with $m_2\geqslant 28$ is less than 5% and for surfaces where $m_2\geqslant 11$ it is less than 10%. The exact expressions for roughness factor of various power-law spectra can be obtained by substituting various expressions of m_2 in Sec. II C. R^* for a large roughness cutoff fractal is estimated as

$$R^*\approx\frac{1}{\pi}\sqrt{\frac{1-\rho^{-2(1-H)}}{1-H}}\left(\frac{l}{L_{\min}}\right)^{1-H}. \tag{2.59}$$

Large roughness surfaces have a roughness factor that increases with ρ and l, and decreases with increasing $L_{\min}$. For $\rho\geqslant\rho_1$ [see Eq. (2.41)] the effect of $L_{\max}$ is insignificant on R^*.

R^* for a marginal fractal has a logarithmic dependence in the range $R^*=\sqrt{2\ln\rho}/\pi$. Similarly, for a cutoff Brownian fractal, R^* is inversely proportional to $\sqrt{L_{\min}}$ and increases with an increase in ρ. R^*, for surfaces with $\rho\geqslant\rho_1$, is a nonmonotonic function of the roughness exponent and has a minimum at the critical value $H=H_1$ [see Eq. (2.42)].

The roughness factor for a large m_2 has a scaling region, i.e., length varies with the measuring ruler size (L), between two crossover length scales. The scaling behavior of the roughness factor can be shown to be

$$R^*\approx(\sqrt{T}/\pi\sqrt{1-H})\;1/L^{1-H}, \tag{2.60}$$

where $L_{\max}/L\geqslant\rho_1$ [ρ_1 is defined in Eq. (2.41)].

Another important geometrical quantity for characterizing the arbitrary geometry of an object is the *curvature*. In contrast to the curvature of a pure power-law spectrum, a band-limited power spectrum is a well behaved quantity. In the following discussion we obtain exact results for the mean square curvature and obtain their two limiting scaling behaviors. This method is not exploited for estimating the fractal dimension.

The ensemble average of the curvature is zero, but the MS curvature is nonzero. The mean square curvature is obtained by taking two averages over the Gaussian joint probability density. The MS curvature is obtained as

$$\langle\kappa^2\rangle=(m_4/\sqrt{2m_2})\,\mathscr{U}(\tfrac{1}{2},-\tfrac{3}{2},1/2m_2). \tag{2.61}$$

The MS curvature increases as the fourth moment of the power spectrum (m_4), but decreases with an increase in ms slope. The slope-dependent factor, i.e., $(1/\sqrt{2m_2})\;\mathscr{U}[\frac{1}{2},-\frac{3}{2},(1/2m_2)]$, varies between 1 and 0. The small-m_2 asymptotic expansion for the MS curvature [see Eq. (A3)] is given by

$$\langle\kappa^2\rangle\sim m_4[1-3m_2]. \tag{2.62}$$

For very small m_2 the MS curvature is asymptotically equal to the fourth moment of the power spectrum (m_4). A numerical comparison of Eq. (2.62) with an exact expression in Eq. (2.61) finds that it underestimates Eq. (2.61) for all m_2. The deviation involved in this approximation for MS curvature is less than 5.2% for $m_2\leqslant 0.06$ and less than 10.7% for $m_2\leqslant 0.09$.

The leading dependence of the MS curvature for large roughness surfaces (i.e., large m_2) is given by

$$\langle\kappa^2\rangle\approx(3\sqrt{\pi}/8)m_4/\sqrt{2m_2}. \tag{2.63}$$

This expression is compared (numerically) with Eq. (2.61) and it is observed that Eq. (2.63) always overestimates the MS curvature. The deviation in estimating Eq. (2.61) by Eq. (2.63) is less than 5% for $m_2>3$ and less than 10% for $m_2\geqslant 1.5$.

The exact expression for the MS curvature can be obtained by substituting the appropriate expressions for m_2 and m_4 (see Sec. II C) in Eq. (2.61). The MS curvature for a cutoff fractal with very *small* m_2 is given by

$$\langle\kappa^2\rangle\approx\frac{1-\rho^{-2(2-H)}}{2\pi(2-H)}\,\frac{1}{l^2}\left(\frac{l}{L_{\min}}\right)^{2(2-H)}. \tag{2.64}$$

The MS curvature increases with a decrease in $L_{\min}$ and increase in ρ. The scaling behavior of MS curvature between two crossover scales is given by

$$\langle\kappa^2\rangle=[T/2\pi(2-H)]1/L^{2(2-H)}, \tag{2.65}$$

where $L_{\max}/L\geqslant\rho_1$ [see Eq. (2.41)]. Equation (2.65) can be used to estimate the roughness exponent for the small-m_2 surfaces or curves.

The leading term in MS curvature of *large* roughness cutoff fractals is given by

$$\langle\kappa^2\rangle\approx\frac{3}{16}\,\frac{\sqrt{1-H}}{2-H}\,\frac{1-\rho^{-2(2-H)}}{\sqrt{1-\rho^{-2(1-H)}}}\,\frac{1}{l^2}\left(\frac{l}{L_{\min}}\right)^{3-H}. \tag{2.66}$$

Equation (2.66) indicates that the MS curvature increases with a decrease in the roughness exponent for given values of the other parameters, e.g., $\langle\kappa^2\rangle_{H\to 1}<\langle\kappa^2\rangle_{H=1/2}<\langle\kappa^2\rangle_{H\to 0}$ for $L_{\min}<l$. The MS curvature increases with a increase in ρ and decreases with a decrease in $L_{\min}$. The scaling behavior of the MS curvature between two crossover scales is given as

$$\langle\kappa^2\rangle\approx[3T\sqrt{1-H}/16(2-H)](1/L^{3-H}), \tag{2.67}$$

where $L_{\max}/L\geqslant\rho_1$. This equation can be used to estimate the roughness exponent for a large-m_2 surface.

E. Zero density and persistence

In this section we obtain an exact result for the mean density of zeros in zero set [41] and its effect on the persistence of a fractal curve. This method has not been used for estimating fractal dimension.

The mean zero crossing density ($\langle N_0 \rangle$) is given by the ratio of the MS slope (or second moment) and the MS width (or zeroth moment) of the surface profile $\zeta(x)$ [30,43]:

$$\langle N_0 \rangle = (1/\pi)\sqrt{m_2/m_0}. \tag{2.68}$$

The mean distance between consecutive zeros is approximately written as

$$\langle d_0 \rangle \approx 1/\langle N_0 \rangle. \tag{2.69}$$

Substituting expressions for the moments of the cutoff fractal in Eq. (2.68), we obtain the zero crossing density as

$$\langle N_0 \rangle = \frac{1}{\pi}\left(\frac{H}{1-H}\right)^{1/2}\left(\frac{1-\rho^{-2(1-H)}}{1-\rho^{-2H}}\right)^{1/2}\frac{1}{L_{\min}^{1-H}L_{\max}^{H}}. \tag{2.70}$$

The $L_{\min}^{1-H}L_{\max}^{H}$ factor in Eq. (2.70) can be looked upon as a generalized geometric mean of the two cutoff scales. $H=1/2$ corresponds to the ordinary geometric mean, where equal weight is given to two cutoff scales. $H>1/2$ corresponds to the case where more weight is given to the upper cutoff scale. Such a surface has a greater mean distance between consecutive zeros compared to a Brownian fractal, which means that the sub-Brownian fractal has a persistent surface profile. Similarly, $H<1/2$ corresponds to a case where the lower cutoff scale has higher weight and such a surface has a smaller mean distance between consecutive zeros (higher zero density) than a Brownian fractal does, which means that the super-Brownian fractal has antipersistence in its surface profile. So the Hurst exponent is a measure of persistence in the surface profile.

In Eq. (2.70), $\langle N_0 \rangle$ decreases for sub-Brownian fractals but increases for super-Brownian fractals with a increase in range. This is shown in Fig. 7, where we have plotted the logarithm of the relative mean zero density, which is the ratio of the mean zero density for a Brownian cutoff fractal and mean zero density of an arbitrary cutoff fractal. The parameter values are the normalization constant $T=1$ and the wave-number cutoffs $K_{\max}=\pi$ and $K_{\min}=K_{\max}/\rho$, where the various values of ρ in the curves are 10^2, 10^4, 10^6, and 10^8. This plot for $\langle N_0 \rangle_{1/2}/\langle N_0 \rangle_H$ is equal to 1 for a Brownian cutoff fractal and partitions the figure into persistent and antipersistent regions. Sub-Brownian fractal curves or surfaces fall under the persistence category. Fractals under this category try to maintain their trends so they make less frequent zero crossings. Contrarily, super-Brownian fractals fall under antipersistence category. Fractals under this category try to oppose the trend so they make more frequent zero crossings. Persistence and anti-persistence behavior becomes stronger with an increase in the range of cutoff scales.

The scaling behavior of $\langle N_0 \rangle$ for a surface with finite fractality between two crossover lengths is given by

$$\langle N_0 \rangle = [\sqrt{H/1-H}/\pi L_{\max}^{H}]\ 1/L^{1-H}, \tag{2.71}$$

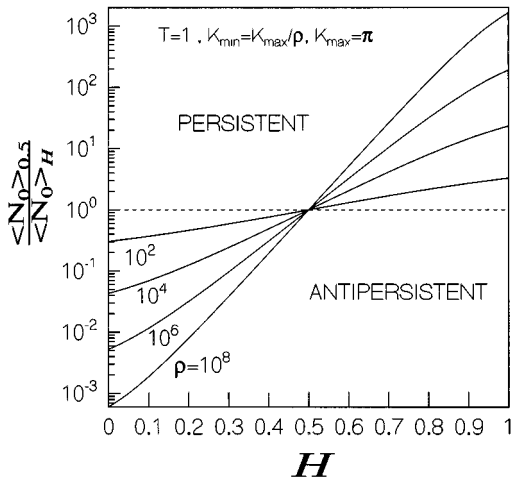

FIG. 7. Plot of the mean zero crossing density [Eq. (2.70)] $\langle N_0 \rangle_{H=1/2}/\langle N_0 \rangle_H$ versus the Hurst exponent H. The parameter values are the normalization constant $T=1$ and the wave-number cutoffs $K_{\max}=\pi$ and $K_{\min}=K_{\max}/\rho$, where the various values of ρ in the curves are 10^2, 10^4, 10^6, and 10^8. We see that the Hurst exponent H is the measure of persistence and antipersistence and these tendencies increase with an increase in the range of cutoff scales.

where $L_{\max}/L \geqslant \max[\rho_0,\rho_1]$. Equation (2.71) can be used to estimate the scaling exponent.

Results for the mean density of extremum points show that it increases with a decrease in the Hurst exponent of a cutoff fractal. So surfaces with a lower Hurst exponent look rougher than those with a higher Hurst exponent. In the limit $L_{\min}\to 0$ one obtains a space filling surface. The results for the mean number of the zeros of a higher derivative or, in general, the r-th derivative of a random surface $\zeta(x)$ per unit horizontal length are available from the author.

III. GRANULAR FLOW EXPERIMENTS

The flow of granular materials, such as sand, shows a rich variety of rather astonishing and poorly understood phenomenon. The flow of sand has recently attracted considerable interest [44–52] and this flow can be looked upon as the random time series for density [48,51,52] or stress fluctuations [49,50]. These time series are $1/f^{\alpha}$ noise with a low frequency white noise [49–53].

To give a better understanding as an approximately self-affine time series and to characterize various time scales involved in the problem of flowing sand in a hopper we compare our theoretical results with experiments. We use the experimental data of Baxter *et al.* [50] for the flowing sand. In their work they measured the stochastic time series for the stress difference between the two spatial locations exerted by the flowing sand on the wall of a hopper. The power spectrum of Ref. [50] is approximated by various forms given in Sec. II A and an approximate fit for the third power spectra is shown in the inset of Fig. 8, where various parameters are $T=7.19\times 10^6, H=0.565$, $\beta=0.05$, $K_{\min}=0.4\pi$, and $K_{\max}=500\pi$. Solid symbols in Fig. 8 show the SF of the experimentally recorded data of Baxter *et al.* and curve (V) is the second-order polynomial fit to logarithmic data. In Fig. 8 we have plotted various theoretical structure functions, viz.,

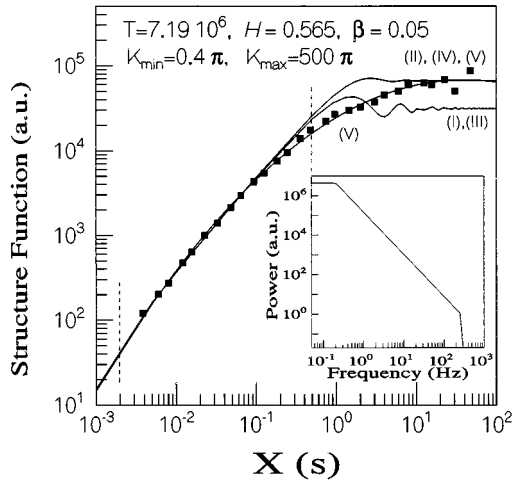

FIG. 8. Plot of the power spectrum and the structure function for a stochastic time series for the stress exerted by the flowing sand on the wall of a hopper. The inset shows an approximate fit to the power spectrum of Ref. [50] and the fit parameters are $T=7.19\times10^6$, $H=0.565$, $\beta=0.05$, $K_{\min}=0.4\pi$, and $K_{\max}=500\pi$ [see Eq. (2.5)]. Solid symbols show an experimental structure function of Ref. [50] and curve (V) is obtained by fitting a second-order polynomial to the logarithm of these data points. Curves (I)–(IV) are theoretical structure function [see Eqs. (2.11) and (2.20)–(2.24)] plots obtained under various approximations for the fitted power spectra and curves (I)–(IV) indicate the subscript of SFs obtained in the text. Vertical bars denotes the approximate scaling region obtained using Eqs. (2.32) and (2.33). We see that the experimental time series is an approximately self-affine fractal.

$\Delta_{\rm I}$, $\Delta_{\rm II}$, $\Delta_{\rm III}$, and $\Delta_{\rm IV}$. These theoretical curves for structure functions fit well with the experimentally measured SF. The structure functions (I) and (III) underestimate experimental SFs for the large scales, whereas the curves (II) and (IV) for SFs are good for large separation scales. Another important point to note in Fig. 8 is that near the outer crossover scale, all theoretical curves overestimate the SF. This is because power spectra used in our calculations overestimate power close to $K_{\min}$ due to a sharp transition to white noise spectra. The oscillation in theoretically calculated SFs originates from the sharp change in power spectra.

Two crossover time scales in this problem are $L_i=0.0019$ and $L_o=0.4959$. Between these time scales the time series shows an approximate self-affine evolution. For time scales longer than L_o the system shows long time saturation behavior where the SF is equal to the twice the variance [see Eq. (2.17)]. Similarly, for time scales smaller than L_i the system approximately evolves in a quadratic way [see Eq. (2.15)].

In Table I we tabulate expected values of various statistical gross measures for the sand flow experiment of Ref. [50]. In column I we tabulate gross numerical values of various statistical measures for power spectra given by Eq. (2.3), in column II we tabulate the power spectra given by Eq. (2.4) and in column III we tabulate the power spectra of Eq. (2.5). In this table we show the quantitative trends caused by the inclusion of contribution of low wave-number non-power-law spectra and high-wave-number non-power-law spectra on the gross value of statistical measures.

We use the definitions of all quantities as defined in the text of this paper, which differ from those used in Ref. [50] e.g., one-half of m_0 in this paper is equal to MS fluctuation of Ref. [50] . This discrepancy occurs due to a different definition used for the Fourier transform of the data.

TABLE I. Various statistical quantities calculated from the expressions obtained for the three power spectra in this paper. The parameters are $T=7.19\times10^6$, $H=0.565$, $\beta=0.05$, $K_{\min}=0.4\pi$, and $K_{\max}=500\pi$.

Statistical quantities	I	II	III
m_0	3.12×10^4	6.65×10^4	6.65×10^4
m_2	3.16×10^7	3.16×10^7	3.32×10^7
m_4	2.37×10^{13}	2.37×10^{13}	2.79×10^{13}
R^*	4.49×10^3	4.49×10^3	4.59×10^3
$\langle\kappa^2\rangle$	1.98×10^9	1.98×10^9	2.28×10^9
$\langle N_0\rangle$	10.1	6.9	7.1

From Table I one can see that the contribution from the low-frequency nonfractal crossover is important for the statistical properties such as m_0 and $\langle N_0\rangle$. Similarly, the contribution from the high frequency nonfractal crossover is important for the value of m_2, m_4, R^*, $\langle\kappa^2\rangle$, and $\langle N_0\rangle$. The numerical value of the moments grows with the order of the moment. It is surprising to note that the Schaeffer-Pitman frequency ($f_s=U/L^*\beta^*\approx10$ Hz) for instability is approximately equal to the mean zero crossing density ($\langle N_0\rangle$) of the time series. Here U and $L^*(\sim10$ cm) are the characteristic velocity and length scales for the experiment and $\beta^*(\sim10^{-2})$ is a plasticity theory parameter [49]. f_s increases with an increase in the flow rate, which implies a decrease in the Hurst exponent H and/or an increase in ρ for $\langle N_0\rangle$ (see Sec. II E and Fig. 7). Behringer and Baxter's experiments [49] show such a decrease in the Hurst exponent with an increase in the flow rate. This raises an important question for future investigation to find how the Schaeffer-Pitman frequency is related to the mean zero crossing density of the stress difference time series and a more detailed analysis of experimental data in this regard would be interesting.

IV. CONCLUSION

The aim of this paper is to analyze the statistical properties of corrugated surface fractals and time series with a band-limited power-law spectrum. These band-limited power-law spectra generate approximately self-affine scaling surfaces with analytic properties. Other important conclusions are the following.

(i) We show the existence of approximate scale invariance properties for the various (roughness) statistical measures between two fractal crossover scales, viz., the inner crossover scale (L_i) and the outer crossover scale (L_o). This work unravels the effect of the (spectral) Hurst exponent (H) and the lower ($L_{\min}$) and upper ($L_{\max}$) cutoff scales on various gross roughness features.

(ii) The height correlation function has two nonfractal limits, one for small separation and another for large separation. Similarly, it is shown that the height difference correlation function goes to zero for small separation and for large

TABLE II. Scaling exponent ϕ for various statistical measures.

Statistical measure	m_0	m_2	m_{2r}	R^* large m_2	$\langle\kappa^2\rangle$ small m_2	$\langle\kappa^2\rangle$ large m_2	$\langle N_0\rangle$
ϕ	$-2H$	$2-2H$	$2r-2H$	$1-H$	$2-2H$	$3-H$	$1-H$

separation it approaches $2h^2$ in an oscillatory manner. Power-law behavior is observed as the leading term in the fractal limit (intermediate scales), which is an indicator of statistical self-affine scaling.

(iii) L_i is always greater than $L_{\min}$ and decreases with an increase in H. L_o is always less than $L_{\max}$ and is a nonmonotonic function of H. The range of fractality (ρ_f) is always less than the range of power-law spectra cutoff scales (ρ). It has a maximum value for $H\approx 0.59$. ρ_f is zero for the marginal ($H\to 1$) and extreme ($H\to 0$) fractals, which means that there is no self-affine scaling regime for these fractals with finite bandwidth spectra.

(iv) The leading contribution to the MS width (h^2) comes from $L_{\max}$, though the contribution of $L_{\min}$ is important for the super-Brownian surface fractals ($H<\frac{1}{2}$). The importance of $L_{\min}$ in h^2 is decided by a range ρ_0. We also show that the MS width is a nonmonotonic function of H with a minimum at H_0.

(v) Unlike the MS width, the dominant contribution to the MS slope (m_2) comes from $L_{\min}$. The dependence on $L_{\max}$ contribution is significant for a narrow bandwidth and for sub-Brownian surface fractals ($H>\frac{1}{2}$). The importance of $L_{\max}$ in m_2 is decided by a range ρ_1. The nonmonotonic dependence of the MS slope on H is emphasized by showing a minimum at H_1. The higher moments of power spectra do not possess any critical behavior.

(vi) The roughness factor (R^*), i.e., dimensionless area or contour length, shows two regimes, one scaling and another nonscaling. R^* increases with a decrease in $L_{\min}$ and an increase in ρ. It has a minimum at H_1.

(vii) The MS curvature increases with an increase in m_4 and a decrease in m_2. It shows two scaling regimes.

(viii) The mean zero crossing density ($\langle N_0\rangle$) for the cutoff self-affine fractals is proportional to the generalized geometric mean of the two cutoff scales. $\langle N_0\rangle$ decreases with the Hurst exponent. The mean distance between consecutive zeros reveals that the surface has persistent and antipersistent behavior for sub-Brownian and super-Brownian fractals, respectively. These tendencies increase with the range of fractals.

(ix) For a system close to a Brownian fractal, the finite range correction for evaluating the Hurst exponent is not very important. For such cases the use of the ideal fractal assumption [Eq. (2.1)] for extracting H is justified. But if we are dealing with a system with H sufficiently small or large compared to $\frac{1}{2}$, we need to correct for the cutoff scales [use one of the expressions given by Eqs. (2.26), (2.27), or (2.28)].

(x) The suitability of various formulas depends upon the value of the Hurst exponent of the system. The scaling form for h^2 is suitable for the higher value of H, i.e., $H\gtrsim 0.2$ for $\rho\sim 3\times 10^3$. The scaling formulas for the slope [Eq. (2.43)], curve length [Eq. (2.60)], and curvature [Eq. (2.67)] are suitable for the system with a lower value of H, i.e., $H\lesssim 0.8$ for $\rho\sim 3\times 10^3$. Equation (2.71) for the mean zero crossing density is suitable for the intermediate value of H, i.e., $0.2\lesssim H\lesssim 0.8$ for $\rho\sim 3\times 10^3$. It is important to note that the scaling form for the second [Eq. (2.43)], and higher [Eq. (2.49)] derivatives or curvature [Eq. (2.65] are suitable for all values of H. The scaling exponents for the power-law representation ($L^{-\phi}$) of various statistical measures between two crossover scales are tabulated in Table II.

(xi) We offer a qualitative explanation for the Sayles-Thomas observation [5] for the distribution of the roughness exponent with dominant intermediate values.

(xii) Results offer a better understanding of the experiments involving granular flow in a hopper than previous works, particularly that of Baxter *et al.* [49,50]. We show that the stochastic time series of their experiment can be looked upon as an approximately self-affine fractal with two crossover time scales. The Shaeffer-Pitman scale and the mean zero crossing density of the observed time series may be related (equal) to each other.

We hope that the results presented here will be helpful to experimentalists engaging in measuring statistical properties of random surface fractals and fractal time series in refining their estimates and will stimulate efforts for precise and further measurements. The approximately self-affine fractal is an important model in the theoretical understanding of various interfacial phenomena. Some of these interesting problems such as diffusion, adsorption of polymers, free energies of fractal membranes in solution and wetting of fractal interfaces are planned to be discussed in the future.

ACKNOWLEDGMENTS

It is a pleasure to acknowledge Sriram Ramaswamy and Rahul Pandit for keen interest and encouragement and Pinaki Majumdar and D. Gaitonde for carefully going through this manuscript.

APPENDIX: USEFUL EXPANSIONS

The small-z expansion for the incomplete gamma functions [36] is

$$\Gamma(a,z)=\Gamma(a)-z^a\sum_{n=0}^{\infty}\frac{(-z)^n}{(a+n)n!}. \tag{A1}$$

The large z-asymptotic expansion for the incomplete gamma function [36] is

$$\Gamma(a,z)\sim z^{a-1}e^{-z}\left[1+\frac{a-1}{z}+\frac{(a-1)(a-2)}{z^2}+\cdots\right]. \tag{A2}$$

The asymptotic expansion of for the confluent hypergeometric function $\mathcal{U}(a,b,z)$ for large z [36] is given by

$$\mathcal{U}(a,b,z)=z^{-a}\sum_{n=0}\frac{(a)_n(1+a-b)_n}{n!}(-z)^{-n}. \quad \text{(A3)}$$

Using the Whittaker function representation of $\mathcal{U}(a,b,z)$ and the small argument [42] expansion for the Whittaker function, we obtain

$$\mathcal{U}(\tfrac{1}{2},2,z)=\frac{e^{z/2}}{z}\mathcal{W}_{1/2,1/2}(z)$$

$$=\frac{-1}{\Gamma(\frac{1}{2})\Gamma(-\frac{1}{2})}\left[\sum_{n=0}^{\infty}\frac{\Gamma(n+\frac{1}{2})}{n!(1+k)!}(z)^n[\psi(n+1)\right.$$

$$\left.+\psi(n+2)-\psi(n+\tfrac{1}{2})-\ln z]-\frac{\Gamma(-\frac{1}{2})}{z}\right]. \quad \text{(A4)}$$

[1] B. B. Mandelbrot, *The Fractal Geometry of Nature* (Freeman, New York, 1982).
[2] J. Feder, *Fractals* (Plenum, New York, 1988).
[3] M. V. Berry, J. Phys. A **12**, 781 (1979).
[4] M. Goulian, N. Lei, J. Miller, and S. K. Sinha, Phys. Rev. A **46**, R6170 (1992).
[5] R. S. Sayles and T. R. Thomas, Nature (London) **271**, 431 (1978); M. V. Berry and J. R. Hannay, *ibid.* **273**, 573 (1978).
[6] P. Meakin, Prog. Solid. State. Chem. **20**, 135 (1990).
[7] J. F. Gouyet, M. Rosso, and B. Sapoval, in *Fractals and Disordered Systems*, edited by A. Bunde and S. Havlin (Springer-Verlag, Heidelberg, 1991).
[8] B. B. Mandelbrot and J. W. van Ness, SIAM Rev. **10**, 422 (1968); J. Llosa and J. Masoliver, Phys. Rev. A **42**, 5011 (1990).
[9] B. B. Mandelbrot, Phys. Scr. **32**, 257 (1985); B. B. Mandelbrot, in *Fractals in Physics*, edited by L. Pietronero and E. Tosatti (North-Holland, Amsterdam, 1986).
[10] P. Pfeifer and D. Avnir, J. Chem. Phys. **79**, 3558 (1983); D. Avnir, D. Farin, and P. Pfeifer, *ibid.* **79**, 3566 (1983).
[11] J. M. William and T. P. Beebe Jr., J. Phys. Chem. **97**, 6249 (1993).
[12] B.B. Mandelbrot, D.E. Passoja, and A.J. Paullay, Nature (London) **308**, 721 (1984); Ma Zhenyi *et al.*, J. Mater. Res. **6**, 183 (1991); M. V. Mitchell and D. A. Bonnell, *ibid.* **5**, 2244 (1990).
[13] J. B. Bates, Y. T. Chu, and W. T. Stribling, Phys. Rev. Lett. **60**, 627 (1988).
[14] I. M. Fuks, Radiophys. Quantum Electron. **26**, 865 (1983).
[15] T. H. Bell, Jr., Deep-Sea Res. **26A**, 65 (1978).
[16] O. M. Phillips, J. Fluid Mech. **4**, 226 (1958); V. E. Zakharov and N. N. Filonenko, J. Appl. Mech. Tech. Phys. **8**, 62 (1967); W. J. Pierson, Jr. and L. Moskowitz, J. Geophys. Res. **69**, 5181 (1964); S. Elgar and G. Mayer-Kress, Physica D **37**, 104 (1989); M. Y. Stiassnie *et al.*, *ibid.* **47**, 341 (1991).
[17] A. N. Kolmogorov, C. R. Acad. Sci. USSR **30**, 299 (1941); S. Chen *et al.*, Phys. Fluids A **5**, 458 (1993); S. Panchev, *Random Functions and Turbulence* (Pergamon, Oxford, 1971); A. S. Monin and A. M. Yaglom, *Statistical Fluid Mechanics* (MIT Press, Boston, 1971).
[18] T. Higuchi, Physica D **31**, 277 (1988).
[19] A. R. Osborne and A. Provenzale, Physica D **35**, 357 (1989).
[20] T. Higuchi, Physica D **46**, 254 (1990).
[21] N. P. Greis and H. S. Greenside, Phys. Rev. A **44**, 2324 (1991).
[22] J. Theiler, Phys. Lett. A **155**, 480 (1991).
[23] A. R. Osborne and A. Pastorello, Phys. Lett. A **181**, 159 (1993).
[24] O. I. Yordanov and N. I. Nickolaev, Phys. Rev. E **49**, R2517 (1994).
[25] S. G. Talocia, Phys. Lett. A **200**, 264 (1995).
[26] J. Theiler, J. Opt. Soc. Am. A **7**, 1055 (1990).
[27] R. F. Voss, Phys. Rev. Lett. **68**, 3805 (1992); H. E. Stanley, Physica A **186**, 1 (1992).
[28] J. R. Womersley and M. R. Hopkins, *Journées des Etats de Surface* (Editions de l'office Professionnel Général de la Transformation des Métaux, Paris, 1945), p. 135.
[29] M. S. Longuet-Higgins, Philos. Trans. R. Soc. London Ser. A **249**, 321 (1957); M. S. Longuet-Higgins, *ibid*. **250**, 157 (1957).
[30] S. O. Rice, in *Selected Papers on Noise and Stochastic Processes*, edited by N. Wax (Dover, New York, 1957).
[31] P. R. Nayak, Trans. ASME **93F**, 398 (1971).
[32] P. Beckmann and A. Spizzichino, *The Scattering of Electromagnetic Radiation from Rough Surfaces* (Pergamon, London, 1963).
[33] D. J. Whitehouse and J. F. Archard, Proc. R. Soc. London **73**, 1 (1966).
[34] J. Peklenik, Proc. Inst. Mech. Eng. (London) Part 3 **183K**, 108 (1967).
[35] T. R. Thomas, Wear **33**, 205 (1975).
[36] *Handbook of Mathematical Functions*, edited by M. Abramowitz and I. A. Stegun (Dover, New York, 1970).
[37] W. Feller, *An Introduction to Probability Theory and Its Application* (Wiley, New York, 1957), Vol. II
[38] D. Labate, F. Canavero, and A. DeMarchi, Metrologia **31**, 51 (1994).
[39] C. G. Fox, Pure Appl. Geophys. **131**, 211 (1989).
[40] P. Grassberger and I. Procaccia, Physica D **9**, 189 (1983).
[41] R. F. Voss, in *Dynamics of Fractal Surfaces*, edited by F. Family and T. Vicsek (World Scientific, Singapore, 1991).
[42] I. S. Gradshteyn and I. M. Ryzhik, *Tables of Integrals, Series and Products* (Academic, San Diego, 1980).
[43] A. Papoulis, *Probability, Random Variable and Stochastic Processes*, 2nd ed. (McGraw-Hill, New York, 1984).
[44] H. M. Jaeger and S. R. Nagel, Science **255**, 1523 (1992).
[45] G. W. Baxter, R. P. Behringer, T. Fagert, and G. A. Johnson, in *Two Phase Flows and Waves*, edited by D. D. Joseph and D. G. Schaeffer (Springer, New York, 1990).
[46] E. B. Pitman and D. G. Schaeffer, Commun. Pure Appl. Math. **40**, 421 (1987).
[47] D. G. Schaeffer, J. Diff. Eq. **66**, 19 (1987).
[48] G. W. Baxter, R. P. Behringer, T. Fagert, and G. A. Johnson, Phys. Rev. Lett. **62**, 2825 (1989).
[49] R. P. Behringer and G. W. Baxter, in *Granular Matter: An*

Interdisciplinary Approach, edited by A. Mehta (Springer-Verlag, Berlin, 1994).
[50] G. W. Baxter, R. Leone, and R. P. Behringer, Europhys. Lett. **21**, 569 (1993).
[51] K. L. Schick and A. A. Verveen, Nature **251**, 599 (1974).
[52] G. H. Ristow and H. J. Herrmann, Phys. Rev. E **51**, 1745 (1995).
[53] G. Peng and H. J. Herrmann, Phys. Rev. E **50**, R5 (1994).